International Conference on Applied Energy 2019
Aug 12-15, 2019, Västerås, Sweden
Paper ID: 581

DEVELOPMENT OF MULTIFUNCTIONAL ADDITIVE COMBINED ELECTROSPUN CARBON NANO FIBERS INTEGRATED BIMETALLIC COPPER COBALT PHOSPHIDE AS AN INTERFACIAL LAYER FOR HIGH-PERFORMANCE DSSC

Fang-Sian Lin [a], Mani Sakthivel [b], Miao-Syuan Fan [b], Jiang-Jen Lin [a, c*], Ru-Jong Jeng [a, d*] and Kuo-Chuan Ho [a, b, c*]

[a] Institute of Polymer Science and Engineering, National Taiwan University, Taipei 10617, Taiwan

[b] Department of Chemical Engineering, National Taiwan University, Taipei 10617, Taiwan

[c] Department of Materials Science and Engineering, National Chung Hsing University, Taichung 40227, Taiwan

[d] Advanced Research Center for Green Materials Science and Technology, National Taiwan University, Taipei 10617, Taiwan

[*]Corresponding Author
E-mail: jianglin@ntu.edu.tw; Fax: +886-2-3366-5237; Tel: +886-2- 3366-5312
E-mail: rujong@ntu.edu.tw; Fax: +886-2-3366-5237; Tel: +886-2- 3366-5884
E-mail: kcho@ntu.edu.tw; Fax: +886-2-2362-3040; Tel: +886-2-3366-3020

ABSTRACT

This study developed a star-shaped 3,6-Bis(5-(4,4′-bis(3-azidopropyl)-[1,1′:3′,1′-terphenyl]-5′-yl)-thien-2-yl)-2,5-bis(2-ethylhexyl)pyrrolo[3,4-c]pyrrole-1,4(2H,5H)-dione (**DPPTPTA**) additive in combination with electrospun carbon nano fibers integrated bimetallic copper-cobalt phosphide **(DPPTPTA/CuCoP/CNF)** as an interface layer for dye-sensitized solar cells (DSSCs). This interface layer is different from conventional blend films. As a multifunctional additive, **DPPTPTA** provides ladder-like energy levels for efficient charge separation, changing the morphology of the interface layer and improving performance. The **CuCoP/CNF** has high electrocatalytic activity and enhanced ionic conductivity. The interface layer ensures efficient charge transfer at the electrode/electrolyte interface with lower electron recombination rate in the DSSC, and it is expected that the photoelectric conversion efficiency (η) of the DSSC can be greatly improved under the condition of 1 sun (AM 1.5G, 100 mW cm^{-2}), and the local boundary is constructed through the interface layer. It ensures long-term thermal stability; and it is expected to have higher η under indoor light condition test, which is one of the most promising devices for renewable energy generation.

Keywords: Bimetallic phosphides, conjugated small polymer, dye-sensitized solar cells, electrospun, interface layer, renewable energy

NONMENCLATURE

Abbreviations	
CNF	Carbon nano fibers
CuCoP	Copper-cobalt phosphide
DSSCs	Dye-sensitized solar cells
PtCE	Platinum counter electrode
Symbols	
η	Photoelectric conversion efficiency
V_{OC}	Open-circuit voltage
J_{SC}	Short-circuit current density
FF	Fill factor

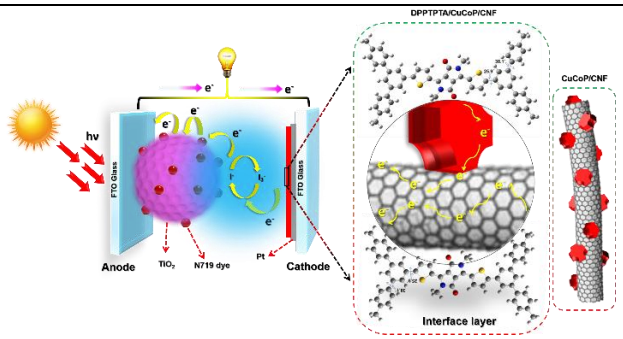

Scheme 1 The working mechanism of **DPPTPTA/CuCoP/CNF** acts as an interface layer in DSSCs.

Selection and peer-review under responsibility of the scientific committee of the 11th Int. Conf. on Applied Energy (ICAE2019).

1. INTRODUCTION

The solar cells provide an effective way to convert the solar energy into electricity directly. Among various kinds of solar cells, the DSSC is especially important in contrast with the conventional solar cells due to its low manufacturing cost [1]. DSSC is comprised mainly of titanium dioxide photoanode (TiO_2) with adsorbed dye molecules, electrolyte containing redox species, and the electrocatalytic platinum counter electrode (PtCE).

Traditionally, liquid electrolyte consists of redox couple (I^-/I_3^-) in organic solvent yields η up to 12%. However, the technological issues due its undesirable intrinsic properties such as solvent evaporation, dye degradation, and leakage affect its long-term stability, which are restrict the commercialization of DSSCs. To solve these problems, several attempts have been made to replace liquid electrolyte with p-type semiconductors, molten salts, organic hole transport materials, and ionic conducting polymers [2]. Nevertheless, the solid state electrolytes show the low electron injection efficiency and the imperfection of filling materials into the nanosized pores of the anode to form a close contact at the interface. Moreover, the absence of solvent leads to deterioration of cell due to the crystallization of salt [3]. To encounter the problems of both liquid and solid electrolytes, the gel polymer electrolytes have been focused intensively due to their stability. However, the gel electrolyte has a low electrolyte load per unit volume and therefore has a low ionic conductivity. Due to the poor interfacial contact, the PtCE/gel polymer interface has a higher resistance than the CE/liquid electrolyte interface for the electrocatalytic reaction of triiodide with reflowed electrons [4]. This leads to a reduction in the overall η. In view of these disadvantages, electrospun polymer membranes activated in ionic liquid electrolytes have been studied for DSSC applications [5].

Here, we propose a multifunctional interface layer that combines the conjugated small molecule **DPPTPTA** and the **CuCoP/CNF** to resolve the problems encountered by the traditional DSSCs mentioned above. A new design for multifunctional additives, namely, **DPPTPTA**, which is easy to synthesize from a diketopyrrolopyrrole (DPP) core. And also, many features to easy synthesis including highly reactive end-capping azido groups and thermal behavior suitable for triggering cross-linking reactions. **DPPTPTA** has a broad absorption wavelength, a favorable absorption intensity, high charge mobility, and a terphenylbased conjugated π-bridge, which can efficiently inhibit molecular aggregation, and induce optimal morphology for the multicomponent system [7]. After incorporating **DPPTPTA** into the interface layer, an enhancement in device performance and thermal stability can be observed [8]. First, some metal compounds exhibit high conductivity (e.g., copper compounds) and some display great electrochemical activity (e.g., cobalt compounds) [9]. Second, the type of anion in metal compounds is another effective agent. By selecting anions with lower electronegativity than oxygen, the electrical conductivity and electrochemical activity of electrodes can be significantly increased [10]. Recently, strong interest has been devoted to the development of transition metal phosphide electrodes for advanced energy storage and conversion applications [11]. Third, an effective approach to enhance the surface area and conductivity is structural engineering. The morphologies that possess nanosized walls with numerous nanopores can provide a high surface area and reduced length for both mass and charge transport [12].

2. EXPERIMENTAL SECTION

2.1 Materials

Lithium perchlorate ($LiClO_4$, ≥98.0%), titanium(IV) tetraisoproproxide (TTIP, >98%), 2-methoxyethanol (99.95%), 3,6-bis(5-bromo-2-thienyl)-2,5-bis(2-hexyldecyl)-2,5-dihydro-pyrrolo[3,4-c]pyrrole-1,4-dione ($C_{46}H_{70}Br_2N_2O_2S_2$, 98%), 4-(4,4,5,5-tetramethyl-1,3,2-dioxaborolan-2-yl)toluene ($C_{13}H_{19}BO_2$), 2-azido-1,3-dimethylimidazolinium hexafluorophosphate ($C_5H_{10}F_6N_5P$, 97%), 1,8-diazabicyclo[5.4.0]undec-7-ene ($C_9H_{16}N_2$, 98%), sodium carbonate (Na_2CO_3, ≥99.0%), diethyl ether (≥99.9%). The 1,4-dioxane (anhydrous, 99.8%), toluene (anhydrous, 99.8%), copper(II) chloride dehydrate ($CuCl_2 \cdot 2H_2O$, ≥99.0%), cobalt(II) chloride hexahydrate ($CoCl_2 \cdot 6H_2O$, 98%) and red phosphorous (≥99.99%) were obtained from Sigma-Aldrich. Lithium iodide (LiI, synthetical grade), poly(ethylene glycol) (PEG, MW~20,000) and iodine (I_2, synthetical grade) were received from Merck. 4-tert-butylpyridine (*t*BP, 96%) and tert-butyl alcohol (*t*BA, 96%) were procured from Acros. 3-Methoxypropionitrile (MPN, 99%) was bought from Fluka.

*2.2 Synthesis of the **DPPTPTA** conjugated small molecule*

The precursor of **DPPTPTA** was synthesized through Suzuki–Miyaura cross-coupling of 3,6-bis(5-bromothien-2-yl)-2,5-bis(2-ethylhexyl)pyrrolo[3,4-c]-pyrrole-1,4(2H,5H)-dione and 3,3′-(5′-(4,4,5,5-tetramethyl-

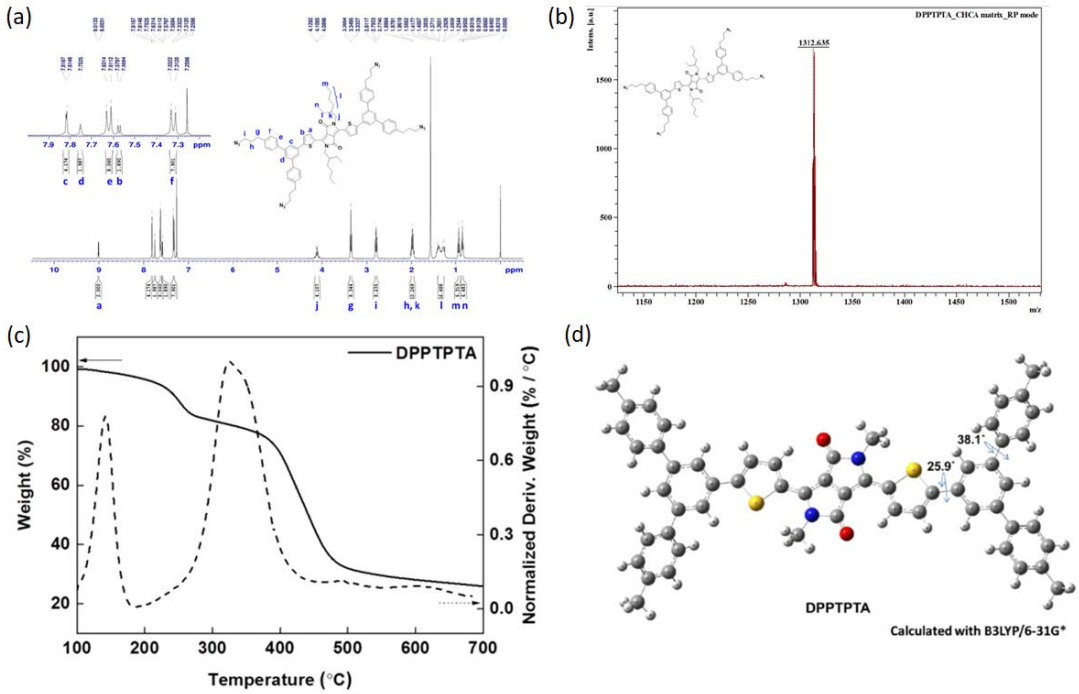

Fig. 1. (a) Chemical positioning determined from FT-NMR spectrum, (b) MALDI-TOF mass spectrum, (c) thermal properties, and (d) optimized structures, calculated with B3LYP/6-31G* theoretical computational models, of **DPPTPTA**.

1,3,2-dioxaborolan-2-yl)-[1,1′:3′,1′-terphenyl]-4,4′-diyl)bis-(propan-1-ol) [13]. **DPPTPTA** was obtained through anazide exchange, reacting with 2-azido-1,3-dimethylimidazolinium hexafluorophosphate (ADMP) and 1,8-diazabicyclo-[5.4.0]undec-7-ene (DBU) [14].

*2.3 Synthesis of **(DPPTPTA/CuCoP/CNF)***

The **DPPTPTA/CuCoP/CNF** was prepared through a single-nozzle electrospinning technique followed by controlled high temperature treatment. In the typical preparation, 1 g of PAN was dissolved in 25 mL of DMF under 80°C. Then 0.75 g of copper(II) chloride dehydrate, cobalt(II) chloride hexahydrate, and red phosphorous were dispersed in 25 mL of DMF for 2 h under magnetic stirring. The dispersed metal precursors were gently added to the homogenous mixture of PAN/DMF solution and conserved with vigorous agitation for 6 h under 80°C to obtain a homogeneous polymer composite precursor. Subsequently, the precursor solution was loaded into a 15 mL plastic syringe equipped with a 21 - gauge blunt tip needle. The flow rate of solution was set to 10 μL min^{-1} by a syringe pump.

The needle was connected to a high - voltage power supply to apply a voltage of 15 kV between the needle and the collector for the formation of nanofibers. The distance maintained between the needle and the collector was 15 cm. Finally, the as-collected film was initially pacified at 80°C for 6 h in an oven and further stabilized at 250°C for 2 h with a heating rate of 10 °C min^{-1}. Followed by carbonization at 900°C for 3 h in N_2 atmosphere with a heating rate of 10 °C min^{-1}, and combined with different concentrations of **DPPTPTA** to prepare the interface layer of DSSCs on PtCE by drop coating.

2.4 Cell assembly

A cleaned FTO glass was coated with a thin compact layer of TiO_2 (100 nm), by using a solution of TTIP in 2-methoxyethanol (weight ratio = 1/3). A TiO_2 film, containing a first layer of transparent layer (10 µm) and a second layer of scattering layer (4 µm) with an active area of 0.20 cm^2 was coated on the treated FTO glass by using a doctor blade technique. The transparent layer was coated on the compact layer using the above-mentioned commercial transparent paste (Ti-nanoxide T/SP), while the scattering layer was further coated on the transparent layer using a home-made scattering paste. Each layer was separately sintered at 500 °C for 30 min in ambient environment. After the sintering process, the TiO_2 film was immersed in a 5×10^{-4} M N719 dye

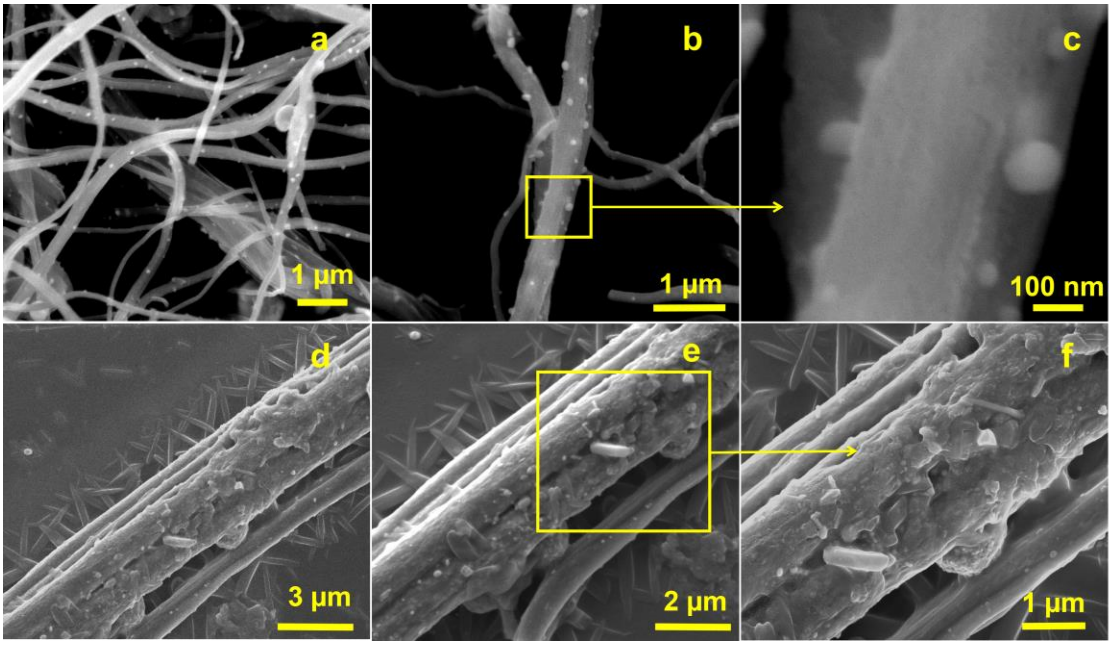

Fig. 2. Different magnified FE-SEM images of (a-c) **CuCoP/CNF** and (d-f) **DPPTPTA/CuCoP/CNF**.

Table 1. Photovoltaic properties of different type of devices in DSSCs.

Type of devices	η (%)	V_{OC} (mV)	J_{SC} (mA cm^{-2})	*FF*	V_{onset} (mV)
Standard device	7.88 ± 0.08	761 ± 2	15.62 ± 0.06	0.66 ± 0.01	520
Bare DPPTPTA	8.53 ± 0.02	793 ± 1	15.86 ± 0.03	0.68 ± 0.00	595
Bare CuCoP/CNF	8.59 ± 0.03	813 ± 1	15.61 ± 0.02	0.68 ± 0.01	608
DPPTPTA/CuCoP/CNF	9.50 ± 0.02	827 ± 2	16.25 ± 0.02	0.71 ± 0.00	655

※ The standard device means without an interface layer.

※ The standard deviation data for each DSSC are obtained based on three cells.

solution for 24 h at room temperature using a mixed solvent of *t*BA and ACN (volume ratio = 1/1).

Thus, a dye-adsorbed TiO_2 film was prepared as the photoanode of a DSSC. Finally, the dye-adsorbed TiO_2 photoanode was coupled with a PtCE with an interface layer, and a cell gap of 25 μm thick Surlyn® film as the spacer. The electrolytes in this study were composed of 0.1 M LiI, 0.05 M I_2, 0.6 M DMPII, 0.5 M *t*BP in ACN/MPN (volume ratio = 8/2). These electrolytes were injected into the cell gap between the two electrodes by capillarity. Finally, a DSSC of a photoanode/electrolyte/interface layer/PtCE is formed.

3. RESULTS AND DISCUSSION

*3.1 Characterization of **DPPTPTA** conjugated small molecule*

The compounds were characterized using elemental analysis, FT-NMR spectroscopy, and matrix-assisted laser desorption/ionization time-of-flight mass spectrometry (MALDI-TOF MS). We assigned the chemical shifts for each proton in the FT-NMR spectra (Fig. 1a) and confirmed the high purity of **DPPTPTA** from its MALDI-TOF mass spectrum (Fig. 1b). Thermogravimetric analysis (TGA) revealed that **DPPTPTA** exhibited two stages of thermal decomposition at 142 and 325 °C; the first involves thermal decomposition of the azido groups and the second characterizes the thermal degradation of the conjugated backbone (Fig. 1c). Theoretical calculations suggested that **DPPTPTA** should possess the large bond-twisting angles (25.9 and 38.1°), and the terphenyl group should induce strong steric effects (Fig. 1d) leading to a low degree of intermolecular stacking. As we had expected, the incorporation of the terphenyl structure

led to the molecular twisting of the DPP derivative. The efficient intermolecular π-stacking of DPP was undermined, so that the resultant **DPPTPTA** exhibits a lower degree of molecular aggregation.

*3.2 Characterization of **CuCoP/CNF***

Fig. 2(a-c) shows the field-emission scanning electron microscope (FE-SEM) images of **CuCoP/CNF**. It suggests that the **CuCoP/CNF** has the uniform three-dimensional interconnected carbon network, whereas the uniform structure of nanoparticle can be observed on the CNF structure. In addition, the integration of **DPPTPTA** with **CuCoP/CNF** is evidently confirmed by using the FE-SEM images (Fig. (d-f)). It shows that the **DPPTPTA** is uniformly covered on the surface of the **CuCoP/CNF** and acts as an interconnected path between the fibers. It facilitates the faster charge carrier conduction to redox couples from the PtCE.

Fig. 3a displays the XRD pattern of **CuCoP/CNF**, copper phosphide, cobalt phosphide, and graphite samples. The obtained XRD pattern of copper phosphide shows the peaks to the standard JCPDS 65-1973. Whereas, the cobalt phosphide exhibited the diffraction peaks, which are matched with JCPDS 65-2381. At the same time, the XRD pattern of graphitic carbon shows only the single peak at 13.09 ° for corresponding plane of (210) related to the JCPDS 8-415 standard data. Finally, **CuCoP/CNF** composite exhibits the combined diffraction peaks of copper phosphide, cobalt phosphide and graphitic carbon. It preliminarily suggests the formation of CuCoP and its integration of graphitic CNF. the XPS study was carried out for the prepared **CuCoP/CNF** and recorded the resultant wide scan and high-resolution spectra for Cu 2p, Co 2p, P 2p and C 1s (Fig. 3b). The wide scan XPS spectra is shown in Fig. 3(c-f) with the characteristic peaks for Cu 2p, Co 2p, P 2p, C 1s and O 1s. It concluded the presence of Cu 2p, Co 2p, P 2p, and C 1s states in **CuCoP/CNF** samples. Meanwhile, the O 1s is ascribed due to the surface contaminants. The Fig. 3c shows the high-resolution XPS spectra of Cu 2p, which exhibits the two peaks for spin-orbital doublets of Cu $2p_{1/2}$ and Cu $2p_{3/2}$ at binding energies of 952.46 and 932.65 eV respectively. Both the doublet peaks contain the mixed electronic states of +2 and +4. Moreover, the two satellite peaks were detected at 942.44 and 962.37 eV. Meanwhile, the XPS spectra of Co 2p deconvoluted into two characteristics peaks of Co $2p_{1/2}$ (796.93 eV) and Co $2p_{3/2}$ (780.84 eV) including the two satellite peaks at binding energies of 786.05 and 802.57 eV respectively (Fig. 3d). The high resolution XPS spectra of P 2p shows in Fig. 3e, from the spectra the peak at 129.377 eV is associated to P $2p_{1/2}$ and P $2p_{3/2}$. Whereas the peak at 132.97 eV is associated to the P due to the exposure of atmosphere air. Besides, the characteristic peaks located at 287.54, 285.55 and 284.95 eV can be ascribed due to the C=C-O, C-O and C-C species respectively (Fig. 3f).

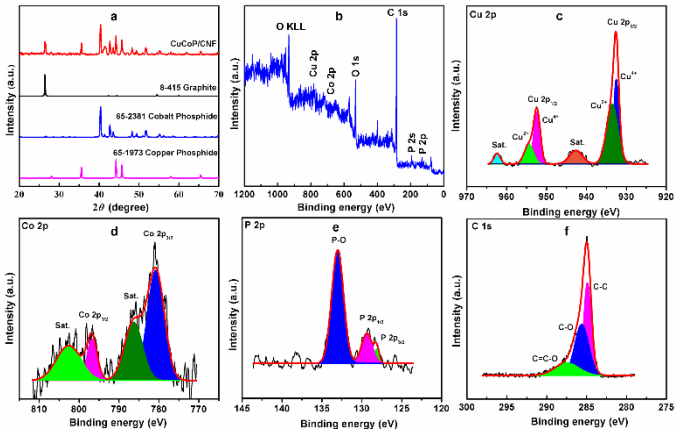

Fig. 3. (a) XRD pattern (b) wide scan XPS (c-f) wide scan XPS spectra of **CuCoP/CNF**.

3.3 Photovoltaic performance of DSSCs with interface layer

The photocurrent density-voltage (*J-V*) curves for a standard DSSC with and without the interface layers obtained under the condition of 1 sun (AM 1.5G, 100 mW cm^{-2}) are shown in Fig. 4, and their corresponding values are given in Table 1. When iodide and polyiodide ions adsorbed on the surface of bimetallic **CuCoP** nanoparticles, the electronic conductivity and surface activity of the interface layer enhanced the charge exchange rate. The interface layer possesses both the advantages of a gel polymer electrolyte as well as the diffusivity of the liquid electrolytes, since its interconnected pore structure can easily entrap an enormous quantity of liquid electrolyte. Thus, the stability of the DSSC with the interface layer is far superior to the conventional DSSC.

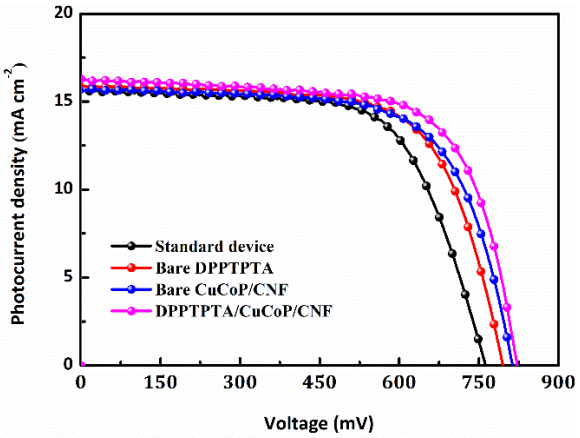

Fig. 4. Current density-voltage curves of the DSSCs with different contents of interface layers measured at 1 sun illumination.

4. CONCLUSIONS

The **DPPTPTA/CuCoP/CNF** is the first application as an interface layer in DSSCs with high ionic conductivity, thermal stability, and good electrochemical properties. The strong interaction between the **DPPTPTA/CuCoP/CNF** and liquid electrolyte induces the space charge layer, which facilitates the fast electron conduction and enhancing the I^-/I_3^- shuttle. In this study, the DSSC combined with **DPPTPTA/CuCoP/CNF** interface layer exhibited the good photovoltaic performance and achieved the highest η of 9.50%. The obtained η is comparatively higher than the standard device without the interface layer (7.88%). Finally, a new type of interface layer was developed in this study. This approach can be used not only in the field dye-sensitized solar cells, but also for the organic solar cells.

ACKNOWLEDGEMENT

This work was financially supported by the "Advanced Research Center of Green Materials Science and Technology" from The Featured Area Research Center Program within the framework of the Higher Education Sprout Project by the Ministry of Education (107L9006) and the Ministry of Science and Technology in Taiwan (MOST 105-2221-E-002-229-MY3, 107-2221-E-002-173-MY3, 107-2218-E-002-001, 107-2119-M-007-001, and 108-3017-F-002-002).

REFERENCE

[1] O'regan B, Grätzel M. A low-cost, High-efficiency solar cell based on dye-sensitized colloidal TiO_2 films. Nature 1991;353:737-740.

[2] Scully SR, Lloyd MT, Herrera R, Giannelis EP, Malliaras GG. Dye-sensitized solar cells employing a highly conductive and mechanically robust nanocomposite gel electrolyte. Synth. Met. 2004;144:291-296.

[3] Shibl HM, Hafez HS, Rifai RI, Abdel Mottaleb MSA. Environmental friendly, Low cost quasi solid state dye sensitized solar cell: polymer electrolyte introduction. J. Inorg. Organomet. Polym. Mater. 2013;23:944-949.

[4] Yuan S, Tang Q, He B, Zhao Y. Multifunctional graphene incorporated conducting gel electrolytes in enhancing photovoltaic performances of quasi-solid-state dye-sensitized solar cells. J. Power Sources 2014;260:225-232.

[5] Zhao J, Jo SG, Kim DW. Photovoltaic performance of dye-sensitized solar cells assembled with electrospun polyacrylonitrile/silica-based fibrous composite membranes. Electrochim. Acta 2014;142:261-267.

[6] Lee YL, Shen YJ, Yang YM. A hybrid PVDF-HFP/nanoparticle gel electrolyte for dye-sensitized solar cell applications. Nanotechnology 2008;19:455201.

[7] Tang B, Liu J, Cao X, Zhao Q, Yu X, Zheng S, Han Y. Restricting the liquid-liquid phase separation of PTB7-Th:PF12TBT:$PC_{71}BM$ by enhanced PTB7-Th solution aggregation to optimize the Interpenetrating network. RSC Adv. 2017;7:17913-17922.

[8] Zhao Y, Li X, Yan B, Xiong D, Li D, Lawes S, Sun X. Recent developments and understanding of novel mixed transition-metal oxides as anodes in lithium ion batteries. Adv. Energy Mater. 2016;6:1502175.

[9] Kaverlavani SK, Moosavifard SE, Bakouei A. Designing graphene-wrapped nanoporous $CuCo_2O_4$ hollow spheres electrodes for high-performance asymmetric supercapacitors. J. Mater. Chem. A 2017;5:14301-14309.

[10] Carenco S, Portehault D, Boissière C, Mézailles N, Sanchez C. Nanoscaled metal borides and phosphides: recent developments and perspectives. Chem. Rev. 2013;113:7981-8065.

[11] Pramanik M, Tsujimoto Y, Malgras V, Dou SX, Kim JH, Yamauchi Y. Mesoporous iron phosphonate electrodes with crystalline frameworks for lithium-ion batteries. Chem. Mater. 2015;27:1082-1089.

[12] Moosavifard SE, El-Kady MF, Rahmanifar MS, Kaner RB, Mousavi MF. Designing 3D highly ordered nanoporous CuO electrodes for high-performance asymmetric supercapacitors. ACS Appl. Mater. Interfaces 2015;7:4851-4860.

[13] Tamayo AB, Dang XD, Walker B, Seo J, Kent T, Nguyen TQ. A low band gap, solution processable oligothiophene with a dialkylated diketopyrrolopyrrole chromophore for use in bulk heterojunction solar cells. Appl. Phys. Lett. 2009;94:103301.

[14] Yue W, Ashraf RS, Nielsen CB, Collado-Fregoso E, Niazi MR, Yousaf SA, Kirkus M, Chen HY, Amassian A, Durrant JR, McCulloch I. A thieno[3,2-b][1]benzothiophene isoindigo building block for additive- and annealing-free high-performance polymer solar cells. Adv. Mater. 2015;27:4702-4707.